FRACTAL-SHAPED COMPLEMENTARY ELECTRIC-LC RESONATOR FOR BANDSTOP FILTER

H.-X. Xu[1, *], G.-M. Wang[1], and Q. Peng[2]

[1]Department of Electromagnetic Field & Microwave Technique, Missile Institute of Air Force Engineering University, Sanyuan 713800, China

[2]School of Foreign Language, Nanchang University, Nanchang 330031, China

Abstract—An equivalent circuit model for single negative metamaterial (MTM) transmission line based on microstrip complementary electric inductive-capacitive resonator (CELC) is proposed for the first time. The verified circuit model gives strong support to the interpretation of all exhibited electromagnetic (EM) phenomena. The nonpure magnetic and electric resonances have been demonstrated by constitutive EM parameters. Based on the conclusions that have drawn, a more compact sub-wavelength particle based on Hilbert-shaped CELC (H-CELC) is proposed. The design procedures of the H-CELC-loaded MTM cell are derived based on the circuit model. For application, a bandstop filter covering one of the ISM bands 5.2 GHz by cascading two H-CELC cells is designed, fabricated and measured. Consistent results between simulation and measurement have confirmed the design. The established theory based on the proposed circuit model is of reference value for the design of novel bandstop devices.

1. INTRODUCTION

Left handed (LH) bulk metamaterials (MTMs), enlightened by Veselago's precursory work [1], have essentially generated much interest since the first experimental demonstration was performed by periodically loading conducting wires (realizing negative permittivity) and split ring resonators (SRR) (realizing negative permeability) [2]. Since resonant-type bulk MTMs typically featured large insertion

loss, narrow band and big volume, etc., there was still a step before its practical application. In this regard, extensive researches have focused on fabricating MTMs to address those drawbacks, e.g., nonresonant-type composite right/left handed transmission line (CRLH TL) MTMs [3], and resonant-type CRLH TL based on complementary split ring resonators(CSRRs) [4] and complementary omega-like structure [5].

Recently, one type of electric inductive-capacitive resonator (ELC) [6] and its complementary counterpart (CELC) [7, 8] has been demonstrated as an electric resonator and a magnetic resonator in bulk MTMs, respectively. However, they exhibited expected response on rigorous requirement of a certain polarization and incident wave excitation. As to the transmission line (TL) MTMs, although a novel CELC had been applied to microstrip phase shifter [9], the unknown working mechanism of CELC and the absence of a circuit model and correlative theory have reduced its technical merits. Moreover, the potential for further miniaturization of the circuit area is still available. Recently, the fractal theory has been widely employed in the design of microwave components [10, 11] and antennas [12, 13] based on its space-filling and self-similarity property which enables the compact or multi-band design. Most recently, the fractal perturbation in single negative (SN) MTM TL by using complementary single split resonator (CSSRR) with an alterative split [14] and complementary ring resonator (CSR) without a split [15] has been proposed by the authors to engineer a more compact sub-wavelength particle.

In this paper, we firstly propose a circuit model for the CELC-loaded SN MTM TL in microstrip technology for circuit analysis and design, followed by a characterization of the magnetic and electric resonances from constitutive electromagnetic (EM) parameters and a systemic research on how different constitutive elements contribute to the establishment of the overall performances of SN MTM TL in Section 2. Inspired by [10–15], a novel Hilbert-shaped CELC (H-CELC) is proposed for a more compact sub-wavelength particle in Section 3, followed by a popularization of it in a bandstop filter (BSF) design. Illustrative results of the BSF including simulation and measurement are also provided. Finally, a major conclusion is highlighted in Section 4. The work in this paper is of practical value in designing controllable magnetic MTMs TL.

## 2. CHARACTERIZATION OF CELC LOADED SN MTM CELL

2.1. Topology and Verification of the Equivalent Circuit Model

The topology of a CELC-loaded SN MTM cell in conjunction with its corresponding lumped-element equivalent circuit model is shown in Figure 1. As can be observed, the cell consists of a signal line in the conductor strip and a CELC etched in the ground plane. CELC is specified by the width of etched slot g, each length of the symmetrical four arms L, and the height of center pole h. Note that the extended long arm in a finite space can be realized by winding it in a spiral shape. The structure is described by means of a circuit model shown in Figure 1(b), where L_s models the line inductance; C_s is composed of line capacitance and coupling effect between the line and CELC; L_g models the inductance induced by the center pole; L_p represents inductance aroused by top/bottom arms. Note that L_g and L_p are not the inductances of the pole and the arm but correspond to the inductive effect produced when current flows along the boundary of the CELC slot. C_p represents the capacitive effect between internal metallic ground and external metallic ground separated by the CELC slot. It is worth to point out that C_p is mainly dependent on the gap distance between the top and bottom arms when the dimension of CELC is fixed and is significant when the gap infinitely decreases or even disappears. R is applied to account for the loss. Identical two shunt branches formed by L_p, C_p and R are considered for the symmetrical effect of CELC. For characterization, the F4B-2 substrate with a thickness of 0.8 mm and a dielectric constant of 2.65 is adopted for full-wave EM simulation which is implemented in commercial MOM-based simulator Ansoft Designer.

To demonstrate the rationality of the proposed circuit model, the sub-wavelength particle is investigated by means of planar EM simulation as well as electrical simulation. During the circuit parameters extraction process (electrical simulation), we have applied the circuit model in commercial circuit simulator Ansoft Serenade to match the magnitude and phase of S-parameters to the EM simulated ones. Figure 2 illustrates S-parameters of the CELC-loaded cell. It is observed that the obtained S-parameters between EM simulation and electrical simulation are in reasonable agreement. Slight discrepancy is mainly due to the wide scope of frequencies that we have observed as any circuit model would deteriorate its merit in describing the EM phenomena of a physical structure when the scope exceeds the appropriate frequency band. A further inspection of these

(a)   (b)
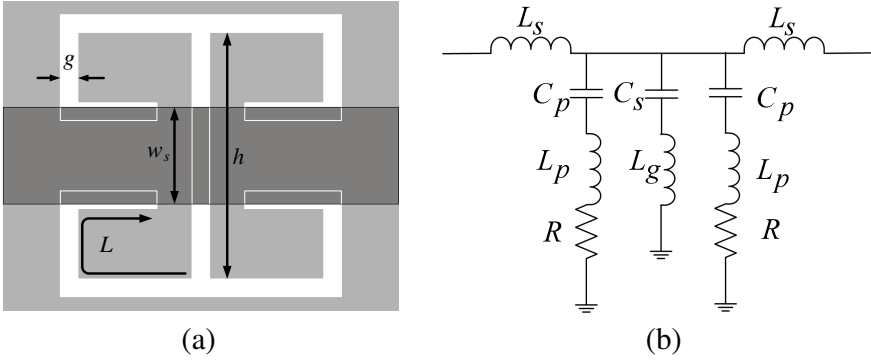
Figure 1. (a) Topology and (b) corresponding lumped-element equivalent circuit model of the SN MTM cell. The CELC (depicted in white) is etched in the ground (depicted in light grey) underneath the conductor strip (depicted in dark grey).

(a)   (b)
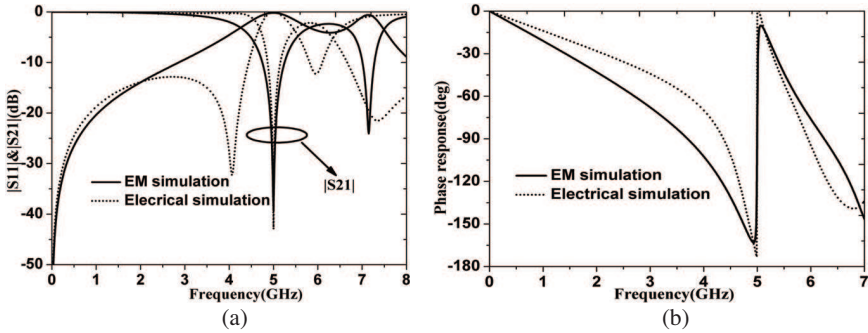
Figure 2. S-parameters of the CELC-loaded SN MTM cell obtained from full-wave EM simulation and electrical simulation. (a) Magnitude response, (b) transmission phase response. The physical parameters of the CELC-loaded cell are: $w_s = 2.2$ mm, $g = 0.2$ mm, $L = 7$ mm, $h = 4.6$ mm, and dimension of the entire cell is 9 mm. Extracted lumped-element parameters are: $L_s = 1.44$ nH, $C_s = 0.12$ pF, $L_g = 8.44$ nH, $L_p = 3.57$ nH, $C_p = 0.13$ pF and $R = 12.3\,\Omega$.

S-parameters reveals that there are obvious two transmission zeros in the frequency band of interest. That is to say, etched CELC inhibits the signal propagation at two resonant frequencies around 5 GHz and 7.2 GHz, respectively.

2.2. Constitutive EM Parameters and Full-Wave S-parameters

To provide a deep insight into the working mechanism, an improved Nicolson-Ross-Weir (NRW) approach using S-parameters developed in [16] by converting the free-space propagation to air-filled microstrip line propagation is applied to the constitutive EM parameters retrieval, in which we adopted a mathematical method proposed by Chen et al. [17] to choose the correct branch of real part of refractive index for robustness. Figure 3 depicts the constitutive EM parameter of the cell. Two most important aspects should be highlighted. First, the negative refractive index (NRI) does not occur all along attributing to a SN permittivity or permeability. Second, there are evident two resonances in the observed frequency band, namely a magnetic resonance in the lower band and by contrast an electric resonance in the upper band. The exhibited phenomenon and working mechanism are certainly unlike those from CELC in bulk MTMs which only responded to the in-plane magnetic fields and in turn showed a pure magnetic response [7]. The fundamental magnetic resonance can be successfully interpreted by the existence of the center pole which can be considered as a complementary component of the conducting wire. According to Babinet's duality principle, the negative permeability of CELC in the vicinity of magnetic resonance is immediately engineered. As to the resultant electric resonance, we will disclose the principle beginning with the circuit analysis.

For convenience, the lossless case is considered. The series impedance and shunt admittance of the circuit model shown in Figure 1(b) are calculated as

$$Z_s = jwL_s, \tag{1a}$$

$$Y_p = 2jwC_p/(1 - w^2L_PC_P) + jwC_s/(1 - w^2L_gC_s). \tag{1b}$$

From (1b), the magnetic and electric resonant frequencies which are the key factor of the resultant two transmission zeros are determined by
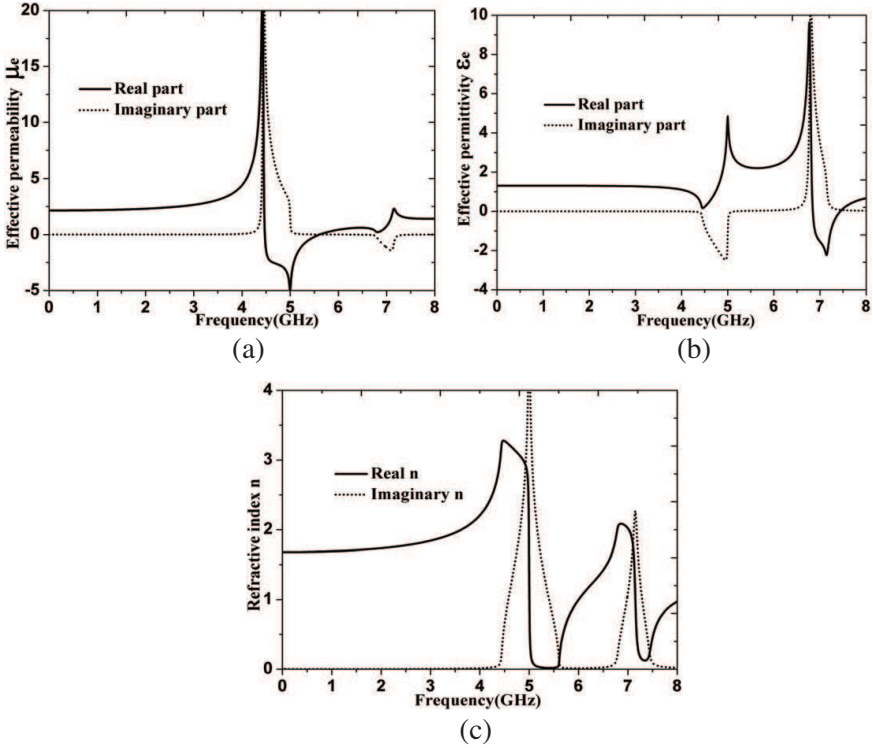
$$f_M = 1\Big/2\pi\sqrt{L_gC_S}, \tag{2a}$$

$$f_E = 1/2\pi\sqrt{L_PC_P}. \tag{2b}$$

The impedance of the cell is formulated as

$$Z = \sqrt{\frac{Z_s}{Y_p}} = \sqrt{\frac{jwL_s(1 - w^2L_PC_P)(1 - w^2L_gC_s)}{/[jwC_s(1 - w^2L_PC_P) + 2jwC_p(1 - w^2L_gC_s)]}} \tag{3}$$

By inserting the retrieved lumped-element parameters (shown in the caption of Figure 2) into (2), two transmission zeros are evaluated

Figure 3. Constitutive EM parameters of CELC-loaded SN MTM cell. (a) Effective permeability, (b) effective permittivity and (c) refractive index.

as 5.01 GHz and 7.39 GHz, respectively ,which are quantitative very similar to those magnetic and electric resonant frequencies obtained from EM simulation. A good agreement of theory and simulation has further verified the circuit model. We also conclude that the parasitical electric response is attributing to the reactive elements L_p and C_p in the shunt branch formed by the top/bottom arms.

It is of great interest to see how the transmission performance changes with various geometrical parameters of CELC. Figure 4 depicts the comparisons of S-parameters of the cell in different cases. Referring to Figure 4(a), it shows that the magnetic resonance slightly shifts toward higher band while the electric resonance shifting toward lower band as g increases from 0.2 to 0.5 mm because when slot width grows, L_g decreases, and C_p accordingly increases due to the reduction of gap distance between the top and bottom arms. Figure 4(b) depicts the influence of different L on the transmission performance. One
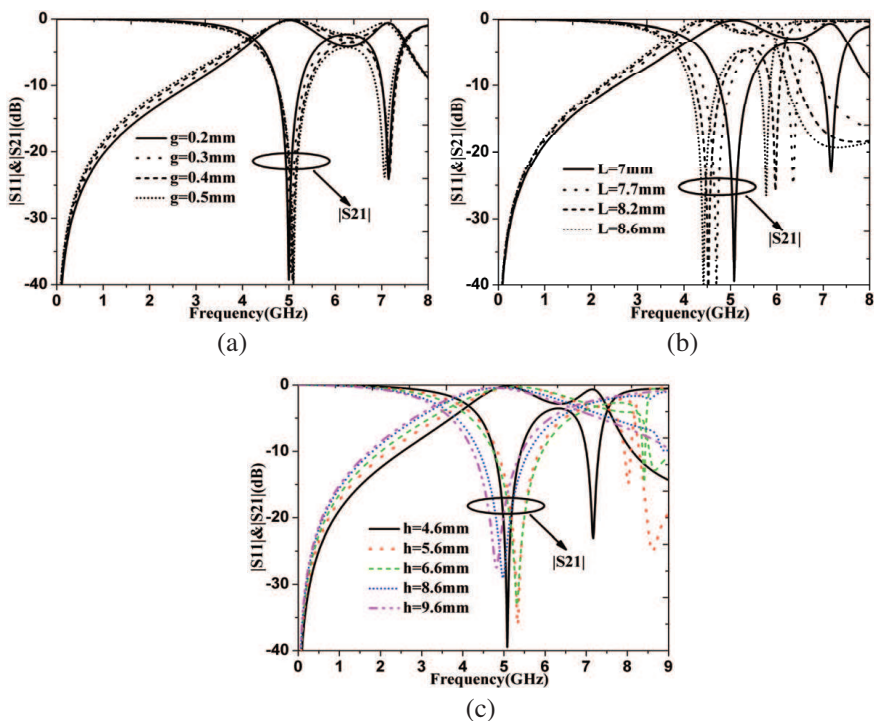
Figure 4. S-parameters of the CELC-loaded SN MTM cell with various geometrical parameters. (a) Various g ($L = 7$ mm, $h = 4.6$ mm), (b) various L ($g = 0.4$ mm, $h = 4.6$ mm), (c) various h ($g = 0.4$ mm, $L = 7$ mm).

may clearly observe that the increase of L from 7 to 8.6 mm causes rapid decrease of both resonances especially the electric resonance. Therefore, the two attenuation poles become closer and even form a stopband as L extends. The extended L in a given occupied area directly increases L_p while indirectly increases L_g. The enhancement of L_p is much stronger than L_g, thus the electric resonance decreases even faster than the magnetic one, and a merged stopband is naturally envisaged. Figure 4(c) illustrates the influence of different h on the transmission characteristic. It is found that the magnetic resonance is almost without a frequency shift, but the electric resonance shifts toward higher band and even vanishes in the observed scope as h increases from 4.6 to 9.6 mm because the extended h increases the gap distance and in turn reduces the value of C_p. Note that although L_g increases as h extends, the coupling between CELC and conductor line decreases, namely C_s decreases. Therefore, a fixed magnetic resonance

is expected according to (2).

In conclusion, the results in Figure 4 afford us a complete understanding of the working mechanism of CELC in microstrip technology. The ability to control the magnetic or electric resonance offers us several degrees of flexibility and good guidelines in practical design of a SN MTM TL with specified operation band and electrical performances. The arm's length can be adjusted for more compact sub-wavelength particle while pure magnetic resonance can be engineered by increasing the pole's height.

3. NOVEL H-CELC-LOADED CELL FOR A BSF

Based on the conclusions that have drawn, we propose a more compact sub-wavelength H-CELC whose top/bottom arms are constructed as Hilbert curve of second iteration order. Figure 5 shows the layout of the proposed H-CELC-loaded SN MTM cell. For characterization, the H-CELC-loaded cell and the forthcoming BSF are fabricated on the F4B-2 substrate with a thickness of 0.8 mm and a dielectric constant of 2.65. Note that although the magnetic and electric resonances can be controlled by adjusting the geometrical parameters, it is impossible to construct the two resonances in the same band to form a LH passband as CELC cannot simultaneously excite two modes. In reverse manner, the magnetic and electric resonances can be engineered infinitely close to each other to form a wide stopband. The design procedures of H-CELC-loaded SN MTM TL are generally described as follows.

First, apply the circuit model depicted in Figure 1 in Ansoft Serenade to synthesize several possible groups of circuit elements through an optimization to engineer a wide stopband with specified
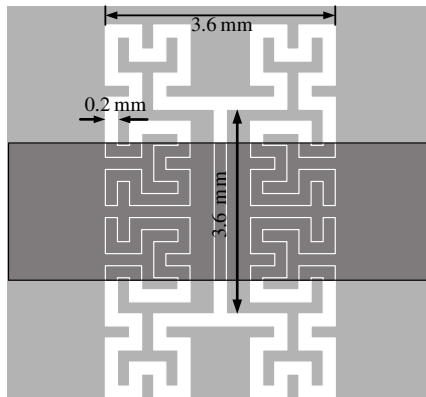
Figure 5. Layout of the proposed SN MTM cell based on H-CELC.

electrical performances, e.g., operating frequency, stopband bandwidth and cut-off frequency, followed by an insertion of the obtained circuit parameters into (2) and (3) to select the correct solution. In this process, f_M and f_E are examined to check whether they are in the target stopband, and Z is applied to check whether it is within an acceptable range around reference impedance $50\,\Omega$ in the passband by a program code in mathematical software Matlab. Second, roughly figure out the layout of H-CELC according to the fixed circuit elements, e.g., the pole's height can be determined mainly according to L_g and C_s. The dimensions of the minimum fractal segment which decides the entire Hilbert fractals can be skillfully optimized referring to L_p and C_p, and the dimensions of conductor line are estimated according to L_s.

Figure 6 plots the simulated results of the designed H-CELC-loaded SN MTM cell. The occupied area of the proposed sub-wavelength particle is only 60% of the CELC-loaded cell operating at the same band. The finite-element (FEM)-based simulator Ansoft HFSS is applied to characterize the current distribution. Consistent S-parameters from Ansoft HFSS and Ansoft Designer have further demonstrated the design. As expected in Figure 6(a), the magnetic resonance is engineered at $5.2\,\mathrm{GHz}$ (ISM band), and electric resonance is implemented adjacent to it. The working mechanism can be interpreted successfully through that fractal perturbation in CELC has significantly extended the arm's length in a given occupied area, which in turn directly increases L_p and indirectly increases L_g as discussed above. From Figure 6(b), we learn that the current flows across the fractal boundary which accordingly extends the current path, and the


(a)   (b)
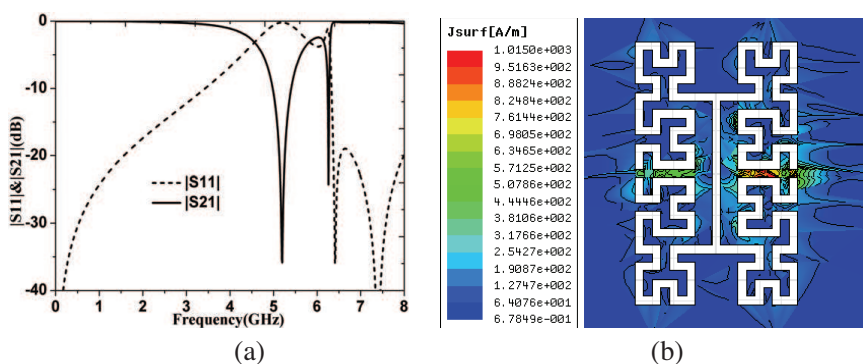
Figure 6. Simulated results of the designed SN MTM cell based on H-CELC. (a) S-parameters obtained from Ansoft Designer. (b) Current distribution from Ansoft HFSS.

current density is sharply enhanced in the gap between the top and bottom arms which further verifies that reduced gap distance enables a large C_p in the derived circuit model.

The bandstop performance of the H-CELC can be applied to design a BSF. In this regard, two cascaded H-CELC cells are symmetrically arranged in the ground to sharpen the rejection skirt and enhance the signal suppression between the magnetic and electric resonances. The utilized open-circuited stub in the conductor line is from the point of view of good impedance match and can be optimized to improve the passband performance accordingly. The H-CELC can be designed following the procedure discussed above. Figure 7 shows the fabricated prototype of the proposed BSF. For verification, the prototype filter is simulated by Ansoft Designer and measured through *Anritsu ME7808A* vector network analyzer. Figure 8 plots the simulated and measured S-parameters of developed BSF. It is obvious that these results are in reasonable agreement except a slight frequency shift in the lower and upper reflection zeros which has confirmed the design. Slight discrepancy is due to the inherent tolerances in the fabrication process. It is also observed that measured return loss $|S_{11}|$ is better than 10 dB in the passband and the suppression at the center frequency 5.2 GHz approximates to 27 dB. The measured bandwidth characterized by insertion loss larger than 3 dB is ranged from 4.5 GHz to 5.9 GHz thus a relative stopband bandwidth of 26.9% relative to 5.2 GHz is engineered.

Compared to the previous U-shaped and V-shaped BSFs [18], the performance of the BSF in this paper is comparable, but the circuit is more compact, and only two cascaded cells are adopted. Thanks to the

(a)   (b)
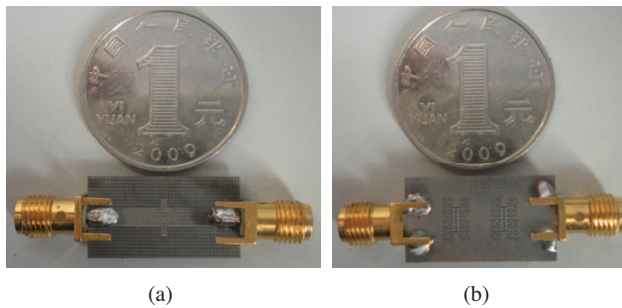
Figure 7. Fabricated prototype of the designed BSF using two cascaded H-CELC cells. (a) Top view and (b) bottom view. The width and height of open stub in the center of conductor strip are 0.8 mm and 5.4 mm, the distance (periodicity) between the two cells is 7 mm.
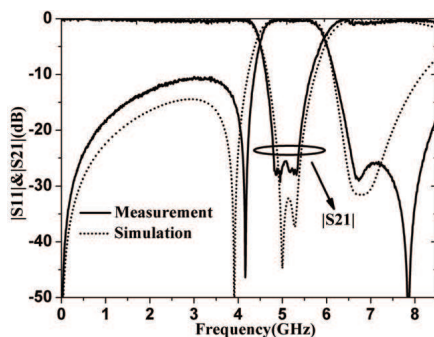
Figure 8. Simulated and measured S-parameters of the proposed BSF.

conjoint magnetic and electric resonance, the rejection skirts of BSF in the lower and upper edge of stopband are steeper than [18]. The measured selectivity is calculated as $63\,\mathrm{dB/GHz}$ (from 4.5 to 4.77 GHz) and $34\,\mathrm{dB/GHz}$ (from 5.4 to 5.9 GHz) in the lower and upper transition band, respectively according to [19]

$$\xi = (\alpha_2 - \alpha_1)/(f_2 - f_1) \tag{4}$$

where α_1 is the 3 dB attenuation point at f_1, α_2 is the 20 dB attenuation point at f_2. A wider stopband and steeper rejection skirt can be obtained if more H-CELC-loaded cells with gradually changed dimensions were adopted as in [14]. The engineered electrically smaller particle by combining the fractal geometry and MTM TL is the major merit of the H-CELC. Therefore, the H-CELC-loaded SN MTM cell can be extensively applied to other devices and antennas design where the compact and harmonics suppression are the major concerns.

4. CONCLUSION

In this work, the rationality of the initially proposed circuit model for CELC-loaded SN MTM cell has been fully demonstrated by full-wave simulation and theory. A systemic characterization of the cell by constitutive EM parameters is performed. Some interesting conclusions are also made, that is, the CELC-loaded MTM TL exhibits an additional electric resonance after the fundamental magnetic resonance which quite differs from the CELC in bulk MTMs with pure magnetic resonance. Moreover, the magnetic resonance is demonstrated mainly dependent on the arm's length while the electric resonance is determined mainly by the distance between top and bottom arms, and the arm's length. By smart application of the two

resonances and fractal geometry, a novel electrically smaller H-CELC with wide stopband is proposed. The improved stopband bandwidth and enhanced selectivity of H-CELC are illustrated by a novel BSF design.

ACKNOWLEDGMENT

REFERENCES

1. Veselago, V. G., "The electrodynamics of substances with simultaneously negative values of ε and μ," *Sov. Phys. Usp.*, Vol. 10, 509–514, 1968.
2. Smith, D. R., W. J. Padilla, D. C. Vier, S. C. Nemat-Nasser, and S. Schultz, "Composite medium with simultaneously negative permeability and permittivity," *Phys. Rev. Lett.*, Vol. 84, 4184–4187, 2000.
3. Caloz, C. and T. Itoh, "Application of the transmission line theory of left-handed materials to the realization of a microstrip 'LH line'," *IEEE AP-S Int. Symp. Dig.*, 412–415, 2002.
4. Falcone, F., T. Lopetegi, M. A. G. Laso, J. D. Baena, J. Bonache, M. Beruete, R. Marque's, F. Martin, and M. Sorolla, "Babinet principle applied to the design of metasurfaces and metamaterials," *Phys. Rev. Lett.*, Vol. 93, 197401, 2004.
5. Messiha, N. T., A. M. Ghuniem, and H. M. El-Hennawy, "Planar transmission line medium with negative refractive index based on complementary omega-like structure," *IEEE Microw. Wirel. Compon. Lett.*, Vol. 18, 575–577, 2008.
6. Schurig, D., J. J. Mock, and D. R. Smith, "Electric-field-coupled resonators for negative permittivity metamaterials," *Appl. Phys. Lett.*, Vol. 88, 041109, 2006.
7. Hand, T. H., J. Gollub, S. Sajuyigbe, D. R. Smith, and S. A. Cummer, "Characterization of complementary electric field coupled resonate surface," *Appl. Phys. Lett.*, Vol. 93, 212504, 2008.
8. Chen, H.-T., J. F. O'Hara, A. J. Taylor, R. D. Averitt, C. Highstrete, M. Lee, and W. J. Padilla, "Complementary planar terahertz metamaterials," *Optics Express*, Vol. 15, 1084–1095, 2007.

9. Lu, M., J. Y. Chin, R. Liu, and T. J. Cui, "A microstrip phase shifter using complementary metamaterials," *Proceedings of International Conference on Microwave and Millimeter Wave*, 1569–1571, Nanjing, China, April 21–24, 2008.

10. An, J., G.-M. Wang, W.-D. Zeng, and L.-X. Ma, "UWB filter using defected ground structure of Von Koch fractal shaped slot," *Progress In Electromagnetics Research Letters*, Vol. 61, 61–66, 2009.

11. Jahanbakht, M. and M. N. Moghaddasi, "Fractal beam KU-band MEMS phase shifter," *Progress In Electromagnetics Research Letters*, Vol. 5, 73–85, 2008.

12. Chen, W.-L., G.-M. Wang, and C.-X. Zhang, "Bandwidth enhancement of a microstrip-line-fed printed wide-slot antenna with a fractal-shaped slot," *IEEE Trans. Antennas Propag.*, Vol. 57, No. 7, 2176–2179, Jul. 2009.

13. Kordzadeh, A. and F. Hojat Kashani, "A new reduced size microstrip patch antenna with fractal shaped defects," *Progress In Electromagnetics Research B*, Vol. 11, 29–37, 2009.

14. Xu, H.-X., G.-M. Wang, and K. Lu, "Tunable low-pass filter using fractal shaped complementary split ring resonator with ultra-wide stop-band and excellent selectivity," *International Conference on Ultra-wide Band Technology*, Vol. 2, 694–696, Sep. 2010.

15. Xu, H.-X., G.-M. Wang, C.-X. Zhang, and J.-G. Liang, "Hilbert-shaped complementary ring resonator and application to enhanced-performance low pass filter with high selectivity," *International Journal of RF and Microwave Computer-Aided Engineering*, Vol. 7, No. 6, 399–406, 2011.

16. Xu, H.-X., G.-M. Wang, and J.-G. Liang, "Novel CRLH TL metamaterial and compact microstrip branch-line coupler application," *Progress In Electromagnetics Research C*, Vol. 20, 173–186, 2011.

17. Chen, X. D., T. M. Grzegorczyk, B.-I. Wu, J. Pacheco, Jr., and J. A. Kong, "Robust method to retrieve the constitutive effective parameters of metamaterials," *Phys. Rev. E*, Vol. 70, 016608, 2004.

18. Woo, D.-J., T.-K. Lee, J.-W. Lee, C.-S. Pyo, and W.-K. Choi, "Novel u-slot and v-slot DGSs for bandstop filter with improved Q factor," *IEEE Trans. Microwave Theory Tech.*, Vol. 54, 2840–2847, 2006.

19. Karmakar, N. C., "Theoretical investigations into binomial distributions of photonic bandgaps in microstrip line structures," *Microw. Opt. Technol. Lett.*, Vol. 33, 191–196, 2002.